

On the Robust Experimental Multi-Degree-of-Freedom Identification of Bolted Joints Using Frequency-Based Substructuring

Preprint (December 19, 2022)

Michael Kreutz*, Francesco Trainotti, Verena Gimpl, Daniel J. Rixen

Technical University of Munich, TUM School of Engineering and Design, Chair of Applied Mechanics, Boltzmannstr. 15, 85748 Garching, Germany

* Correspondence: m.kreutz@tum.de

Keywords Bolted Joints, Experimental Substructuring, Frequency-Based Substructuring, Joint Identification, Substructure Decoupling

Abstract

Modeling joint dynamics is the bottleneck for precise predictive models of machines. Bolted joints are especially relevant due to their common use in mechanical engineering. Stiffness and damping properties of bolted joints are highly influenced by contact parameters (geometry, surface treatment, preload, ...). For high amplitude vibrations, when non-appropriate joint closure is present, even frictional effects can play a role.

Substructuring techniques offer a lean solution for isolating dynamical or quasi-static components of joint dynamics. It may be used for an identification of linearized contact parameters for multiple degrees of freedom (dofs). The main limitation of the method is finding a robust workflow to guarantee a proper controllability and observability of the desired joint dynamics, as well as dealing with disturbance/noise in the measurements.

In this contribution a robust procedure for the identification of a bolted joint using frequency-based substructuring is presented for a contact in an experimental scenario. The dynamics of the joint are isolated from the assembled system using different substructuring techniques treating the joint as a quasi-static or dynamic component. A simple physical model of the joint is parametrized from the experimental joint dynamics. A validation of the methodology is given by using the identified joint parameters on a modified assembled system.

Nomenclature

dof(s)	degree(s) of freedom
FBS	frequency-based substructuring
FRF	frequency response function
VPT(,VP)	virtual point transformation(, virtual point)
\mathbf{u}, \mathbf{f}	measured displacements, forces
\mathbf{q}, \mathbf{m}	virtual displacements, forces
\mathbf{Y}, \mathbf{Z}	receptance, dynamic stiffness matrix
\mathbf{R}, \mathbf{T}	VPT reduction, transformation matrix
\mathbf{B}	signed Boolean matrix
λ	Lagrange multiplier
$\mathbf{K}, \bar{\mathbf{C}}, \mathbf{C}, \mathbf{M}$	stiffness, hysteretic damping, viscous damping, mass matrix
k, c	stiffness, viscous damping
f, Ω	frequency, angular frequency
$*_{A(B, J, AJB, A^*JB)}$	pertaining to substructure $A(, B, J, AJB, A^*JB)$
$*_{u/f}$	pertaining to measured displacements, forces
$*_{q,m}$	pertaining to virtual displacements, forces
$*_{2_A(, 2_B)}$	pertaining to set of dofs $2_A(, 2_B)$
$\tilde{*}$	reconstructed from identified values

1 Introduction

Bolts are common connecting elements in mechanical engineering. The dynamics of joints in general or of bolted joints in particular is a bottleneck in creating precise, predictive models. Identification of joint properties with different boundary conditions (e.g. preload, number of contact elements, load direction, tightening procedure, surface roughness, material pairing, ...) can improve models of systems in an early design stage. It helps in better understanding the dynamic behavior of joints and of jointed system. Ultimately, the dynamic effects of joints can be considered in the design process of machines and structures.

One can devise different techniques to identify joint properties or merely its effect on an assembled system. A possible technique is to measure some transfer paths/frequency response functions of an assembled system with a joint and compare it to a numerical model of the system. Through a model updating step, the joint in the numerical model can be adapted to match the experimentally determined dynamics. In theory, this only needs little experimental measurements and only one model updating step. However, physicality of the joint cannot be guaranteed as the optimization process could mix up the parameters of the complex multi-dof system, leading to an overfitting of the joint properties. This impairs the transferability of the obtained joint properties to other systems and masks the physical understanding of the joint.

Another approach consist in introducing in the procedure a so-called isolation step in order to explicitly separate the joints from the rest of the system. Methods to isolate joint dynamics use dynamic substructuring, see [7]. Dynamic substructuring is concerned with analysis of systems in terms of components/substructures. Structures can be assembled or disassembled using equilibrium of interface forces and compatibility of the interface displacements in different domains, see [19, 20]. In experimental practice, frequency response functions can be measured, which describe linear dynamics with respect to frequency. Thus, for experimental applications, frequency-based substructuring is commonly adopted. An assumption of the mentioned dynamic substructuring methods is time invariance of the system dynamics. In bolted joints, this cannot always be guaranteed due to friction effects or partial joint closure. Nonetheless, under the assumption of small nonlinearities, the identified joint model can be seen as a linearization of the joint in the given operational/loading conditions.

This work presents a workflow for a robust identification of linearized contact parameters for a bolted joint using substructuring techniques. In section 2, the theory for joint identification using frequency-based substructuring (FBS) is presented. The identification procedure is divided into two steps: an isolation and a parametrization step. Section 3 presents the experimental test case. At first, the design of the prototype system, consisting of two flexible bodies connected by a bolted joint, is presented. Then the isolation of the joint dynamics is performed and a simple physical parametrization is applied. The identified joint model is then validated on the original assembly and on a slightly modified assembled system. Finally, the effect of varying the bolt torque, which changes the joint's preload, is assessed. Section 4 gives a conclusion and an outlook to further studies.

2 Theory

A two-step procedure is used in this contribution to identify a bolted joint. In the isolation step, the dynamics of the joint is decoupled from the assembled system using substructure decoupling. In the parametrization step, a simple physical model is used to fit the experimentally identified joint dynamics.

2.1 Joint Isolation

The isolation of the joint is performed using frequency-based substructuring. The methods can be organized by the type of isolation and type of joint model, see table 1, cf. [1]. The isolation step can be based on a primal or a dual decoupling. Primal decoupling uses displacements, dual decoupling uses forces as unknowns in the substructuring procedure. As a natural consequence, it is common to use impedance (dynamic stiffness) for primal disassembly and dynamic compliance (i.e. frequency response functions) for dual disassembly.

Another distinction is made depending on the model assumed for the joint to be identified: "Dynamic" if the joint is a dynamic component, i.e. includes inertia effects inside the joint, and "Quasi-Static" if the joint is a massless compliant component, i.e. it only has stiffness and damping parts.

The setup for joint identification consists of a system with two substructures (A , B), that are connected via one

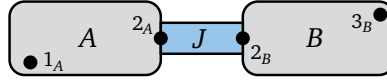


Figure 1: Assembled system with substructures A , B and joint J .

joint (J), see fig. 1. Here, only FRFs that are measured at the interface are used, i.e. at points 2_A , 2_B .

Table 1: Classification of dynamic decoupling methods

	Primal	Dual
Dynamic	Primal Decoupling	Dual Decoupling (LM-FBS)
Quasi-static	Inverse Substructuring	LM-FBS with weakened interface

2.1.1 Virtual Point Transformation

The decoupling and coupling procedures, presented here, require coinciding points at the interface, which cannot be measured directly. Thus, in experimental practice the virtual point transformation (VPT) is often applied, [1, p.126ff], which is described in this section. In analytical models (e.g. finite element models), the conditions can be easily enforced on coinciding nodes. In experiments, it is often not possible to measure all dofs and often not at matching locations. Directly measuring FRFs in rotational dofs is cumbersome. It is very difficult to apply a pure moment to a structure and uncommon to use rotational accelerometers. Also, most of the time, it is not possible to measure directly at the interface, because it is not accessible due to the connection elements like e.g. bolts.

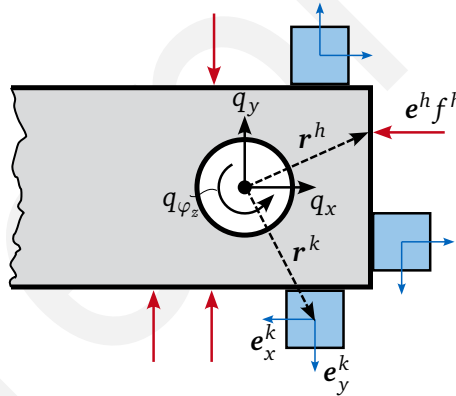


Figure 2: Virtual point transformation.

Thus, it is necessary to project the measurements near the interface to a collocated virtual point. In fig. 2, the virtual point transformation (VPT) is illustrated schematically. The virtual point coordinates \mathbf{q} are obtained from the sensor dofs \mathbf{u} . Similarly the forces and moments \mathbf{m} in the space of the virtual point are obtained from the experimentally applied forces \mathbf{f} . Consequently, the subscript ${}_{uf}$ is used to denote the space of the measurement channels and the subscript ${}_{qm}$ is used to denote the space of the virtual point, e.g. for the transformed FRF \mathbf{Y}_{qm} .

Applying the transformation matrices allows to transform the FRFs from the sensor-space \mathbf{Y}_{uf} to the virtual-point-space \mathbf{Y}_{qm} :

$$\mathbf{Y}_{qm} = \mathbf{T}_u \mathbf{Y}_{uf} \mathbf{T}_f^T. \quad (1)$$

The transformation matrices \mathbf{T}_u , \mathbf{T}_f are obtained from the reduction bases \mathbf{R}_u , \mathbf{R}_f by a Moore-Penrose pseudo-inverse. The pseudo-inverse is denoted by the superscript ${}^+$,

$$\begin{aligned} \mathbf{u} = \mathbf{R}_u \mathbf{q} &\quad \rightarrow \quad \mathbf{q} = (\mathbf{R}_u^T \mathbf{R}_u)^{-1} \mathbf{R}_u^T \mathbf{u} = \mathbf{R}_u^+ \mathbf{u} = \mathbf{T}_u \mathbf{u} \\ \mathbf{m} = \mathbf{R}_f^T \mathbf{f} &\quad \rightarrow \quad \tilde{\mathbf{f}} = (\mathbf{R}_f^+)^T \mathbf{m} = \mathbf{T}_f^T \mathbf{m}. \end{aligned} \quad (2)$$

The reduced force $\tilde{\mathbf{f}}$ describes a minimal forces in a least-squared sense necessary to obtain the resulting forces and moments \mathbf{m} at the interface.

The bases for the projection can be chosen. However, in practice the measurements are often projected using six local rigid modes, which gives the FRFs in the virtual point as translations and rotations. The underlying assumption is that the interface behaves rigidly. It is also possible to include more local “modes” for the interface to account for the flexible motion of the interface. In this contribution, only a rigid basis is used for the VPT so that the virtual point coordinates are given as

$$\mathbf{q} = \begin{pmatrix} \mathbf{q}_t \\ \mathbf{q}_\varphi \end{pmatrix}, \quad \text{with } \mathbf{q}_t = \begin{pmatrix} q_x \\ q_y \\ q_z \end{pmatrix} \quad \text{and} \quad \mathbf{q}_\varphi = \begin{pmatrix} q_{\varphi_x} \\ q_{\varphi_y} \\ q_{\varphi_z} \end{pmatrix}.$$

The generalized forces \mathbf{m} are given in the same directions analogously. It is common to use more channels than the necessary six per dof. Using more channels than necessary makes the problem over-determined. The measurements are projected on the prescribed rigid body modes of the interface in a least-squares sense, see eq. (2). This can mitigate some uncertainties in the measurements.

A detailed derivation of the transformation matrices for the virtual point transformation can be found in [11, 19, 24].

2.1.2 Dynamic Decoupling

Dynamic Decoupling considers the joint as a dynamic component. It removes the dynamic contribution of substructures A and B from the assembled system AJB to isolate the joint J . It requires measuring FRFs of the assembled system and of the individual substructures, and applying the virtual point transformation to obtain \mathbf{Y}_{qm}^{AJB} , \mathbf{Y}_{qm}^A , \mathbf{Y}_{qm}^B , see section 2.1.1. Then, primal or dual decoupling is applied as follows.

Primal Decoupling The FRF-matrices are inverted to obtain the dynamic stiffness matrices $\mathbf{Z}_{qm} = (\mathbf{Y}_{qm})^{-1}$. The decoupling step subtracts the substructures' dynamic stiffnesses from the assembled system's stiffness.

$$\underbrace{\begin{pmatrix} \mathbf{Z}_{2_A,2_A}^J & \mathbf{Z}_{2_A,2_B}^J \\ \mathbf{Z}_{2_B,2_A}^J & \mathbf{Z}_{2_B,2_B}^J \end{pmatrix}}_{\mathbf{Z}_{qm}^J} = \underbrace{\begin{pmatrix} \mathbf{Z}_{2_A,2_A}^A + \mathbf{Z}_{2_A,2_A}^J & \mathbf{Z}_{2_A,2_B}^J \\ \mathbf{Z}_{2_B,2_A}^J & \mathbf{Z}_{2_B,2_B}^B + \mathbf{Z}_{2_B,2_B}^J \end{pmatrix}}_{\mathbf{Z}_{qm}^{AJB}} - \underbrace{\begin{pmatrix} \mathbf{Z}_{2_A,2_A}^A & \mathbf{0} \\ \mathbf{0} & \mathbf{Z}_{2_B,2_B}^B \end{pmatrix}}_{\mathbf{Z}_{qm}^{AB}}. \quad (3)$$

This operation is called Primal Decoupling. In numerical practice, this procedure is well established for the assembly of finite element models.

Lagrange Multiplier-Frequency Based Substructuring The dual formulation of this method is called Dual Decoupling or Lagrange-Multiplier Frequency based Substructuring (LM-FBS), see [8]. This procedure is formulated using directly the FRFs. The coupling or decoupling is enforced via compatibility and equilibrium conditions on the interface.

$$\begin{cases} \mathbf{B}\mathbf{u} = \mathbf{0} \\ \mathbf{u} = \mathbf{Y}(\mathbf{f} - \mathbf{B}^T\boldsymbol{\lambda}) \end{cases} \quad (4)$$

where \mathbf{B} is a signed Boolean matrix that imposes compatibility on the matching interface degrees of freedom (dofs). The matrix \mathbf{Y} includes the matrices of the structures that are to be coupled or decoupled. For joint identification, this is given as

$$\mathbf{Y} = \begin{pmatrix} \mathbf{Y}_{qm}^{AJB} & \mathbf{0} & \mathbf{0} \\ \mathbf{0} & -\mathbf{Y}_{qm}^A & \mathbf{0} \\ \mathbf{0} & \mathbf{0} & -\mathbf{Y}_{qm}^B \end{pmatrix}$$

which indicates decoupling of substructures A and B from the assembled system AJB . Enforcing compatibility and equilibrium yields

$$\mathbf{Y}_{\text{decoupled}}^J = (\mathbf{I} - \mathbf{Y}\mathbf{B}^T(\mathbf{B}\mathbf{Y}\mathbf{B}^T)^{-1}\mathbf{B})\mathbf{Y}$$

The resulting matrix $Y_{\text{decoupled}}^J$ includes the joint FRF, but with redundant dofs. Removing the redundancy in the resulting matrix gives the joint FRF matrix Y_{qm}^J .

From a mathematical point of view primal decoupling and LM-FBS are equivalent methods of dynamic decoupling, when only interface dofs are used, which is the case in this contribution.

2.1.3 Quasi-static Decoupling

Quasi-static decoupling considers the joint as a massless component, e.g. a network of springs and dampers. In the following, two formulations, a primal and a dual, are presented.

Inverse Substructuring Application of quasi-static decoupling in terms of dynamic stiffness is called Inverse Substructuring, cf. [10, 15]. It requires measuring FRFs of the assembled system and applying the virtual point transformation to obtain Y_{qm}^{AJB} , see section 2.1.1.

Consider the dynamic stiffness matrix of the assembled system AJB after inversion:

$$\mathbf{Z}_{qm}^{AJB} = \begin{pmatrix} \mathbf{Z}_{2_A, 2_A}^A + \mathbf{Z}_{2_A, 2_A}^J & \mathbf{Z}_{2_A, 2_B}^J \\ \mathbf{Z}_{2_B, 2_A}^J & \mathbf{Z}_{2_B, 2_B}^B + \mathbf{Z}_{2_B, 2_B}^J \end{pmatrix}$$

It can be seen that the off-diagonal blocks only contain the dynamics of the joint. This can be used to reconstruct the entire dynamic stiffness of the joint. If we assume no cross-coupling between dofs and we further assume the joint to have no mass, i.e. no dynamics, the joint stiffness can be re-constructed as

$$\mathbf{Z}^J = \begin{pmatrix} -\mathbf{Z}_{2_A, 2_B}^J & \mathbf{Z}_{2_A, 2_B}^J \\ \mathbf{Z}_{2_B, 2_A}^J & -\mathbf{Z}_{2_B, 2_A}^J \end{pmatrix}.$$

This identification method is advantageous, because it only requires measuring the assembled system. It is not necessary to measure the individual substructures separately. An equivalent formulation of Inverse Substructuring in the dual domain can be found in [26] and later also improved in [10, 12, 16].

LM-FBS with weakened interface The method LM-FBS with weakened interface in table 1 uses a different formulation in the dual domain, but still identifies a joint as massless, cf. [2]. Compared to inverse substructuring, it additionally requires measuring the FRFs of the individual substructures and transforming the measurements on a virtual point to obtain Y_{qm}^A, Y_{qm}^B . It uses a weakened compatibility condition $\mathbf{B}\mathbf{u} = \Delta\mathbf{u}^J = \mathbf{Y}^J\boldsymbol{\lambda}$ compared to eq. (4). The approach has been presented for joint identification purposes in [9, 13, 22].

In both quasi-static decoupling methods, once the massless joint has been parametrized/identified, it is still possible to take into account of existing mass contributions (e.g. due to bolts, washers, nuts...) by assuming them lumped on the two sides of the interface of components A and B . The relevance of the masses and the lumped approximation will be then validated by reconstructing the assembly AJB (+ masses). This contribution is neglected in the presented work because the mass of the bolt-nut-washer turns out to be small enough compared to the mass of both substructures.

2.1.4 Using Internal Degrees of Freedom

In the presented procedures, only measurement at the interface dofs (dofs labeled "2" in fig. 1) have been used for decoupling. In order to make the decoupling more robust, it can be beneficial to also include internal dofs, i.e. dofs that are not on the interface (dofs labeled "1" and "3" in fig. 1). The additional dynamic information can improve the observability, controllability and conditioning of the interface problem. In [4, 6, 19, 21, 23, 25], extensions of the frequency-based decoupling procedures are presented.

2.2 Joint Parametrization

The joint identification step summarized above yields the dynamic stiffness of the joint as a function of the frequency: $Z^J(\Omega)$. This result could be used directly as a model of the joint. However, this dynamic stiffness can

often polluted by noise and disturbances, thus leading to non-reliable/usable results. It makes sense to extract the joint parameters by fitting the isolated transfer functions following a physical-based modeling approach. A typical example of a physical-based parametrization for a frequency-based identification is

$$Z^J(\Omega) = (-\Omega^2 M^J + j\Omega C^J + (K^J + j\tilde{C}^J))$$

where M^J , C^J , K^J , \tilde{C}^J denote the mass, viscous damping, stiffness and hysteretic damping matrices respectively. The mass matrix M^J would be taken as zero, if a quasi-static joint has been assumed in the isolation step.

The identified model of the joint must be validated. A digital realization of the assembled system is constructed by using the FRF-matrices of the isolated subsystems A and B and the parametrized model for the joint J . This is compared to the direct measurements performed on the assembled system AJB . This is called the validation-step in this contribution. In the cross-validation, the same procedure is performed, but with a slightly modified subsystem A^* . The cross-validation makes a stronger statement about the correctness of the identified joint parameters. It proves the transferability of the joint prediction to other systems with the analyzed contact.

Once a suitable robust procedure is established, it can be used to investigate the joint for changing parameters. For a bolted joint, this can include for example the preload of the bolt due to different torques.

There exist one-step formulations of the proposed joint identification, which are not shown here, but could be found in [5, 18]. These do not separate the joint isolation from the parametrization step, but they try to identify the joint directly from the measured FRFs of the assembly using a model-updating procedure.

3 Experimental Test Case

In this section, the experimental test case is presented.

3.1 Design of the Prototype

The investigated system is given in fig. 3. It consists of 2 substructures (A and B) that are connected via a bolted joint.

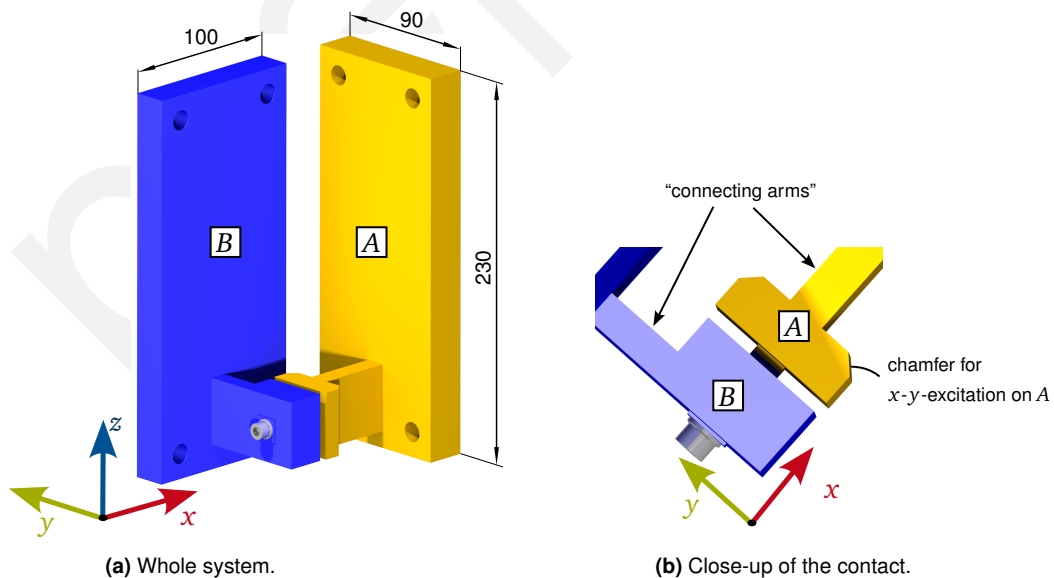


Figure 3: Model of the assembled system AJB .

Substructures A and B are designed to have well separated modes in a medium frequency range below 1000 Hz. This also results in well-separated modes of the assembly. The parts containing the interface are designed as rigid blocks to comply with a rigid virtual point assumption. These interface blocks are connected to the mounting plates via thinner arms. The mounting plates are designed to enable fixing them rigidly to the environment or to use the holes as suspension points for a free-free suspension. In the current design, excitation

in x -direction on substructure A in the assembled system is only possible via chamfers on the interface block, see fig. 3b, due to the size of the commonly used impact hammer. This does not allow excitation purely in the x -direction for substructure A , but in a mixed x - and y -direction. The design of substructure A could be improved by moving the connecting bar closer to the edge of the mounting plate to make excitation in x -direction easier. The structures are made from solid aluminum using CNC milling for easy and repeatable manufacturing. There is no additional surface treatment, even on the interface areas.

A stainless steel M6 bolt and washer is used. Substructure A has a threaded insert. The screw-in depth is about 1.5 times the bolt diameter. The interface surfaces between substructures A and B and between the washer and substructure B at the bolt head are slightly protruding to provide small, well-defined contact areas, see fig. 3b. This will create a high contact pressure and thus ensure defined contact conditions, i.e. full contact in the interface.

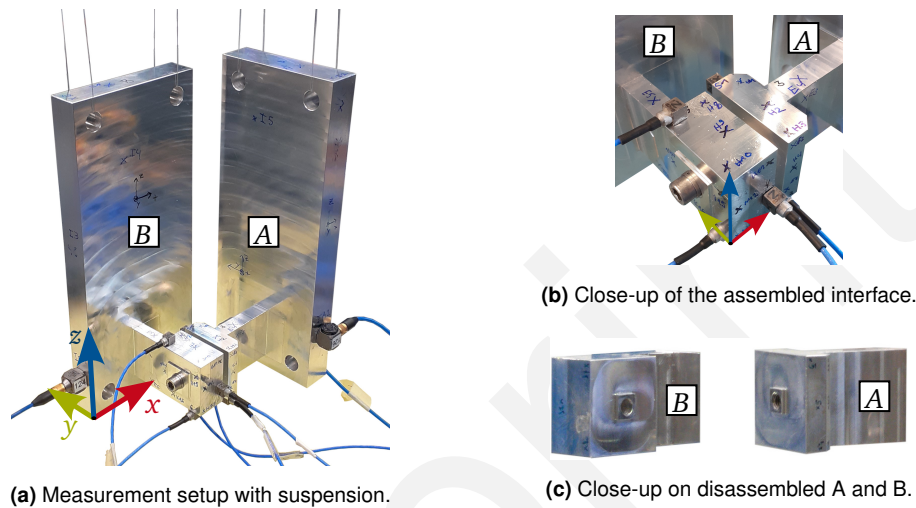


Figure 4: Measurement setup of the assembly.

In the experiments, the individual substructures are investigated with free-free boundary conditions. The parts are suspended with a combination of rubber bands and vinyl wires from a portal frame. On the top of the portal frame rubber bands are used due to their low stiffness, in the lower part of the suspension vinyl wires are used that are looped directly through the mounting plate holes. This provides very low eigenfrequencies of the suspension for a free-free assumption while reducing the movement of the system during testing. A free-free suspension is chosen, because a fixed boundary would be very hard to reproduce between experiments and to parametrize in case a numerical modeling is desired.

On each interface (for each virtual point), three small tri-axial acceleration sensors are used (*PCB 356A03*, range: 500 g, mass $\approx 1 \times 10^{-3}$ kg). The sensors are fixed to the structure using instant adhesive (*Loctite 408*). Additional sensors are attached to the mounting plates, which are not used in this work, but could be used for more advanced decoupling techniques, e.g. using internal dofs, see section 2.1.4. In this work only measurements close the interface are considered.

The structures are excited by an impact hammer with a vinyl tip (*PCB 086C03*). Each impact is adjusted to have a peak force between 100 and 150 N to improve repeatability by avoiding amplitude variations that could lead to nonlinear distortions. Care is taken to distribute the impact points evenly on the interface. Figure 4 shows the measurement setup for the assembled system. Figure 4a shows the setup with the suspension and fig. 4b shows a close-up photo of the interface with the acceleration sensors and some impact position that are marked with crosses.

A *Müller-BBM PAK*-system is used for data acquisition and computing the FRFs. The frequency data is processed using the python-toolbox *pyFBS* [3].

3.2 Isolation

In the isolation step, the dynamics of the joint is decoupled from the system's dynamics. In a quasi-static method, the joint is assumed to only act as stiffness and damping. Here, Inverse Substructuring is used. This is preferred due to its simplicity as it requires only a single measurement campaign on the assembled system. If the joint

presents internal dynamics, i.e. with mass-influence, a dynamic decoupling must be performed. This requires measurements on the assembled system and on the isolated subsystems. Here, Primal Decoupling is used. In order to later validate the quasi-static assumption for the joint model in the inverse substructuring, the authors suggest to compare the results with the joint identification results obtained by a dynamic decoupling approach.

3.2.1 Inverse Substructuring

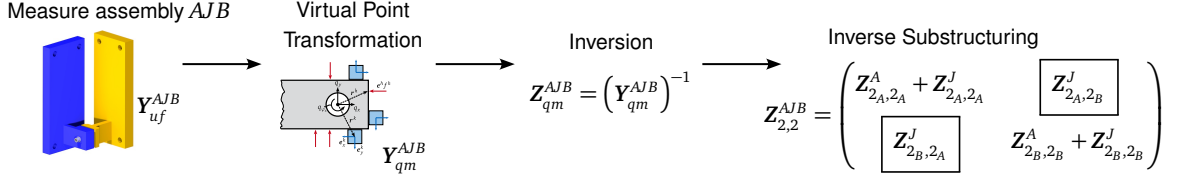


Figure 5: Inverse Substructuring.

Inverse Substructuring uses the dynamic stiffness-matrix of the assembled system: The assumptions are that there is no cross-coupling between connections dofs and no joint dynamics (i.e. no joint mass, see section 2.1.3):

$$Z_{2A,2A}^J = -Z_{2A,2B}^J = -Z_{2B,2A}^J = Z_{2B,2B}^J, \quad Z_{2,2}^J = \begin{pmatrix} -Z_{2A,2B}^J & Z_{2A,2B}^J \\ Z_{2B,2A}^J & -Z_{2B,2A}^J \end{pmatrix}.$$

The upper right and lower left blocks in Z^{AJB} should be the same for an ideal system. In real-life experiments, this is not exactly fulfilled. For this setup, the upper right and lower left blocks agree well, details can be found in fig. 23 of appendix A. For this reason, only entries from the upper right block matrix are shown in this section.

The isolation procedure explained in section 2.1.3 is summarized in fig. 5.

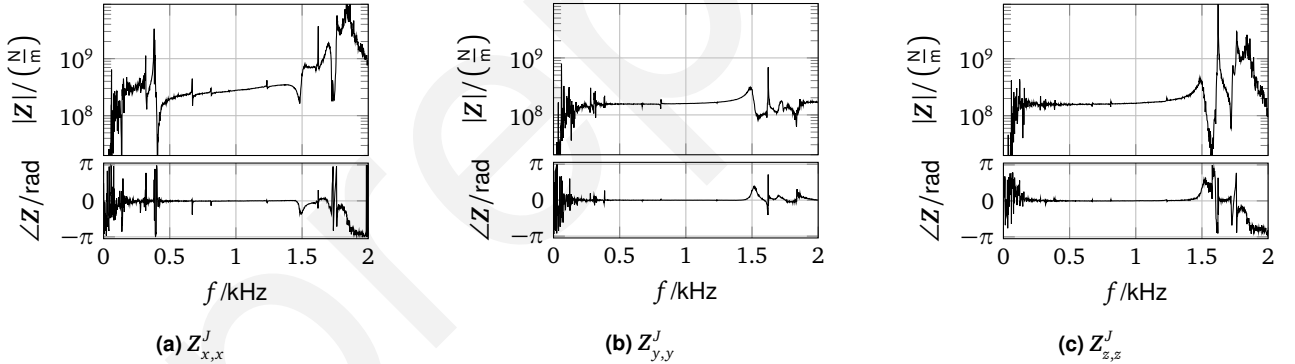


Figure 6: Joint dynamics from Inverse Substructuring for translational dofs.

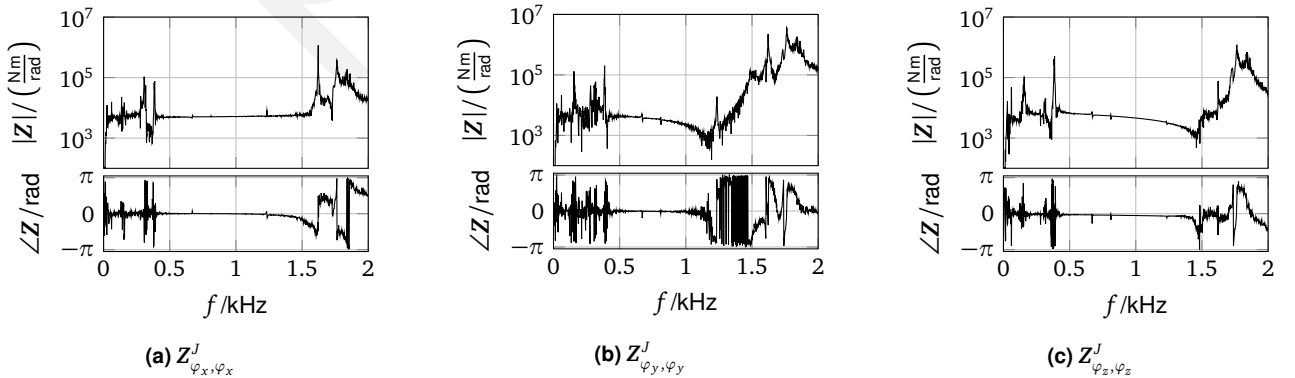


Figure 7: Joint dynamics from Inverse Substructuring for rotational dofs.

Figure 6 shows the isolated direct dynamic stiffness for the translational dofs. Direct stiffness in this sense describes the driving point dynamic stiffness, so for excitation and response in the same direction i.e. values on

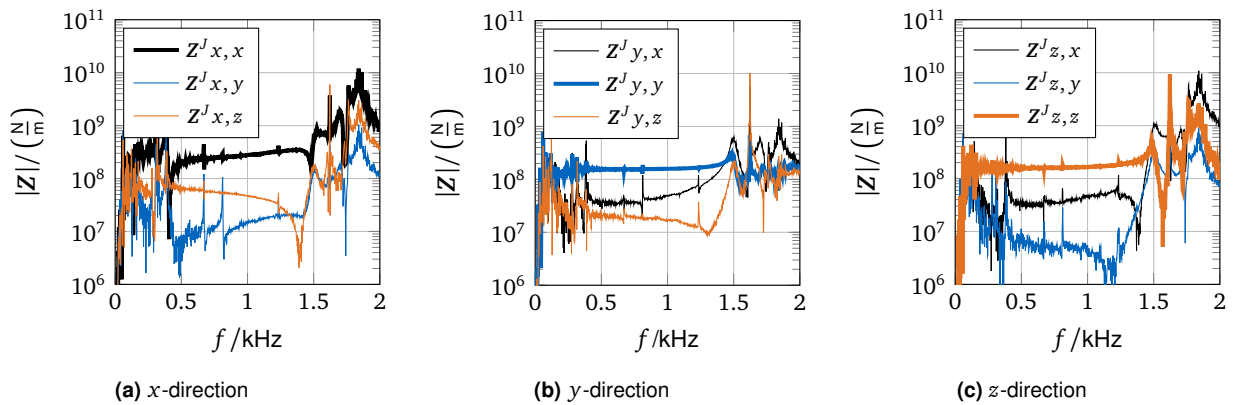


Figure 8: Joint dynamics from Inverse Substructuring for cross-coupling stiffness compared to direct (diagonal) stiffness. Direct stiffness values are drawn as a thick line.

the diagonal of Z_{qm}^J . For the x -direction, in the frequency range between 500 and 1300 Hz the curves are very flat and undisturbed from dynamic peaks/spuriousity. The phase is constant and very close to zero in this region. The results for y and z -direction stiffness are flat in an even larger region than the x -direction stiffness curve. Figure 7 shows the direct dynamic stiffness for the rotational dofs. The rotational stiffness in φ_x has a large flat region like the translational stiffnesses. The directions φ_y and φ_z have a narrower band with flat stiffness highlighting the limited controllability and observability band for these interface DoFs. It is assumed that the dynamics of the joints cannot be well observed in these directions for the current setup. In a parametrization step, only the limited flat regions will be used. The range exhibiting (probably spurious) dynamics

The stiffness curves, shown in figs. 6 and 7, are subject to large disturbances for low frequencies. Results for under 100 Hz are not usable, although the original measured FRFs still have a good coherence in that region. This behavior can be explained by a bad conditioning of the method and the processing in the low frequency region. A similar effect can be seen in rubber joint identification, for example in [10] although not as pronounced as in this case. Indeed, for low frequencies, the assembled system behaves like a rigid body. The joint is not adequately activated and thus cannot be accurately observed. This limitation for the low frequency range is not relevant for the presented methodology, because later in the parametrization step, a constant stiffness and damping will be assumed to be representative for the contact properties (non frequency-dependent behavior), which seems acceptable for the type of joint under analysis, see section 3.3. This procedure is validated in section 3.4.

As explained above, one assumption for Inverse Substructuring is that there is no cross-coupling between the dofs for a given input of the admittance matrix of the joint.. In fig. 8, the magnitude of the translational stiffness are shown. The direct stiffness curves are highlighted with a thick line. The rotational stiffness and the coupling between rotational and translational stiffness are not directly compared. For rotation-translation coupling, the units are different and thus these curves are always hard to compare. More extensive results can be found in fig. 23 of appendix A. It is expected that the cross-coupling terms are order of magnitude lower than the direct stiffness terms: In this figure, it can be seen that the cross-coupling terms are clearly lower than the direct stiffness terms in the relevant flat regions. Only in the regions polluted by spurious dynamics, this is not true. These regions are not used to parametrize the stiffness and thus, do not influence the result. Also, in section 3.4 it can be shown that the system can be well represented even when neglecting the cross-coupling terms.

3.2.2 Comparison with Primal Decoupling

To verify the applicability of the Inverse Substructuring method, its results are compared to the decoupled stiffness using Primal Decoupling. In Primal Decoupling the joint is modeled as a full dynamic component, i.e. it can include mass.

Primal Decoupling requires measurement on the assembled system and additionally also measurements of the individual substructures. The joint stiffness is obtained by subtracting the dynamic stiffness of the substructures from the assembled system, see eq. (3). See fig. 9 for a summary of the procedure.

Comparisons for the results for the translational and rotational dofs are given in figs. 11 and 12. The explanation on how the coefficients are extracted from the joint dynamics matrix is clarified in fig. 10. Both methods use the same set of measurements on the assembled system. This enables a direct comparison without additional sources

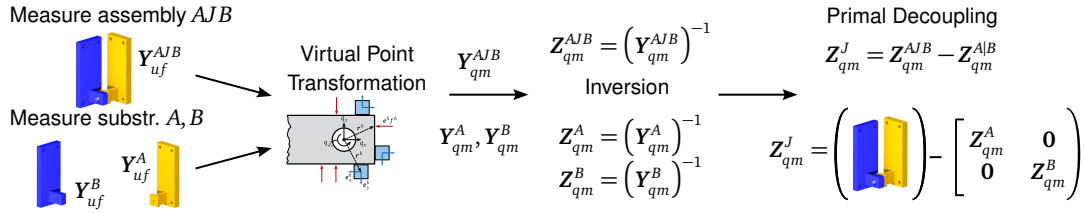


Figure 9: Primal Decoupling.

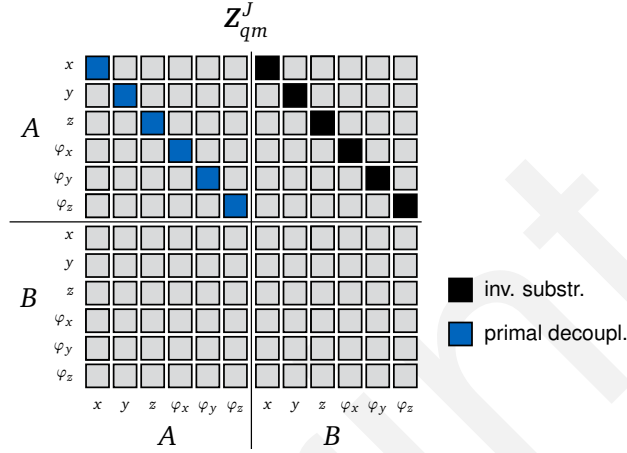


Figure 10: Decoupled joint matrix Z_{qm}^J . Entries in the anti-diagonal blocks are the same as for inverse substructuring. The cells marked in black and blue are shown in figs. 11 and 12.

of inaccuracies/errors due to repeatability of the experiments. The comparisons only show driving point dynamic stiffnesses, i.e. direct stiffnesses $Z_{2_A, 2_A}^J$. The anti-diagonal blocks ($Z_{2_A, 2_B}^J$ and $Z_{2_B, 2_A}^J$) are the same in primal decoupling as in inverse substructuring, because these are not changed by the decoupling.

In the translational dofs, the results from both methods agree very well. For the rotational dofs, there is some difference. In the rotation with φ_x , both methods give good, matching results. The rotation around φ_y does not agree well between the methods. In φ_z , the results agree in a narrow frequency range. As seen in the previous section, section 3.2.1, rotational dynamics have been shown to be more difficult to isolate, especially in φ_y and φ_z directions, which are rotations around axes perpendicular to the bolt axis. As seen above in section 3.2.1 the observability of the rotation is worse than the translations in this setup.

For the translational directions and for the rotation with φ_x , there are again large frequency regions with constant values. This means that the joint does not show dynamic behavior. Also the good agreement between the Inverse Substructuring and the Primal Decoupling further confirms the validity of neglecting the joint dynamics. This means the joint can be reliably modeled by a stiffness and damping contribution in the considered frequency range.

Comparing the experimental effort, inverse substructuring is far superior to primal decoupling as it only requires measurements on the assembled system, but not of the individual subsystems. In this section, it has been shown to give equivalent results. Thus, Inverse Substructuring is the preferred method for isolating the joint dynamics in the presented example.

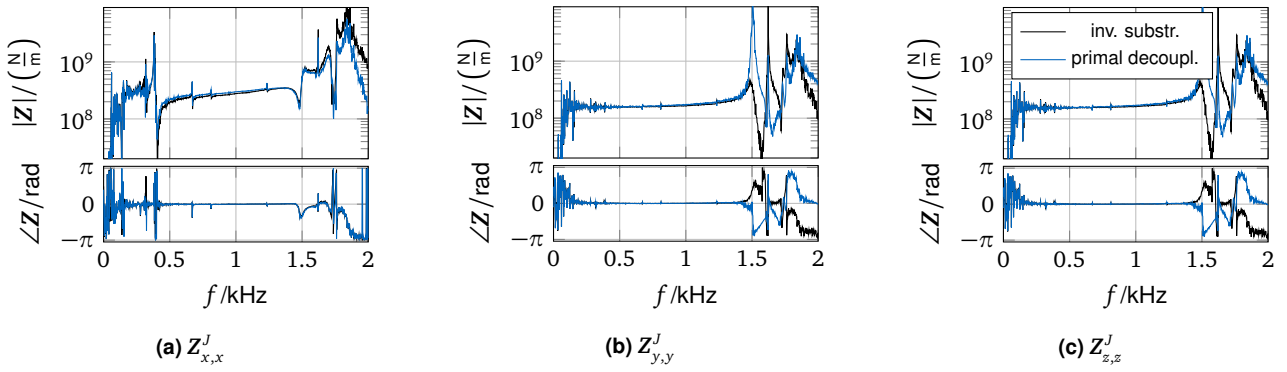


Figure 11: Comparison of isolated joint dynamics from Primal Decoupling and Inverse Substructuring for translational dofs.

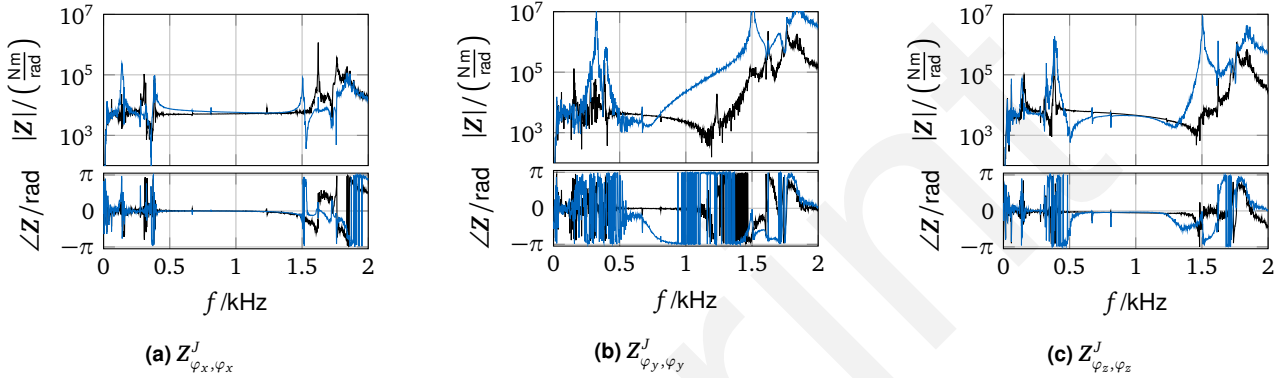


Figure 12: Comparison of isolated joint dynamics from Primal Decoupling and Inverse Substructuring for rotational dofs.

3.3 Parametrization

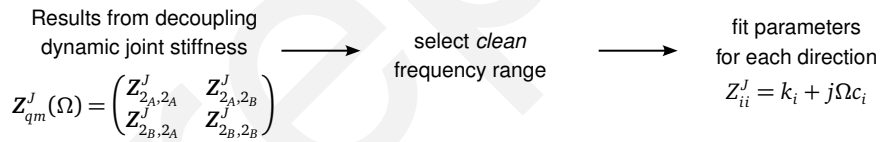


Figure 13: Parametrization: Identification of the parameters of the selected joint model.

The joint is modeled using a classical physical-based approach with stiffness and viscous damping: $Z_{ii}^J = k_i + j\Omega c_i$. The stiffness matrix of the joint is assumed to have only diagonal entries, neglecting cross-coupling between dofs, complying with the assumptions used for Inverse Substructuring.

The procedure for parametrization is given in fig. 13. The parametrization is performed only for the diagonal entries of the dynamic stiffness, for each direction individually. A clean frequency range, without spurious peaks and other dynamic effects, is selected manually, but an automatic procedure could be implemented to make the process more efficient. For the selected region, a least-squares fit (using the python function `scipy.optimize.curve_fit`) is performed fitting separately the real and imaginary parts of each dynamic stiffness Z_{ii}^J .

3.3.1 Parametrization of the stiffness

Figure 14 shows the real part of the decoupled translational stiffness in black. Indicated in orange with horizontal lines is the identified stiffness value for each direction. The translational stiffness perpendicular to the bolt axis (y, z) and the rotational stiffness around the bolt axis (φ_x) can be easily identified because of the large frequency regions with clean real parts. The stiffness values for y and z are similar. This is expected, because the bolted connection is rotationally symmetric around the bolt axis. Thus, the stiffnesses perpendicular to the bolt axis should be equal. The translational stiffness in the bolt axis (x) and the rotational stiffnesses with φ_y and φ_z offer a more challenging identification. It is expected that the stiffness values for φ_y and φ_z should be similar due to the joint's symmetry, which is not validated by the experimental results. This may be due to the poor identification

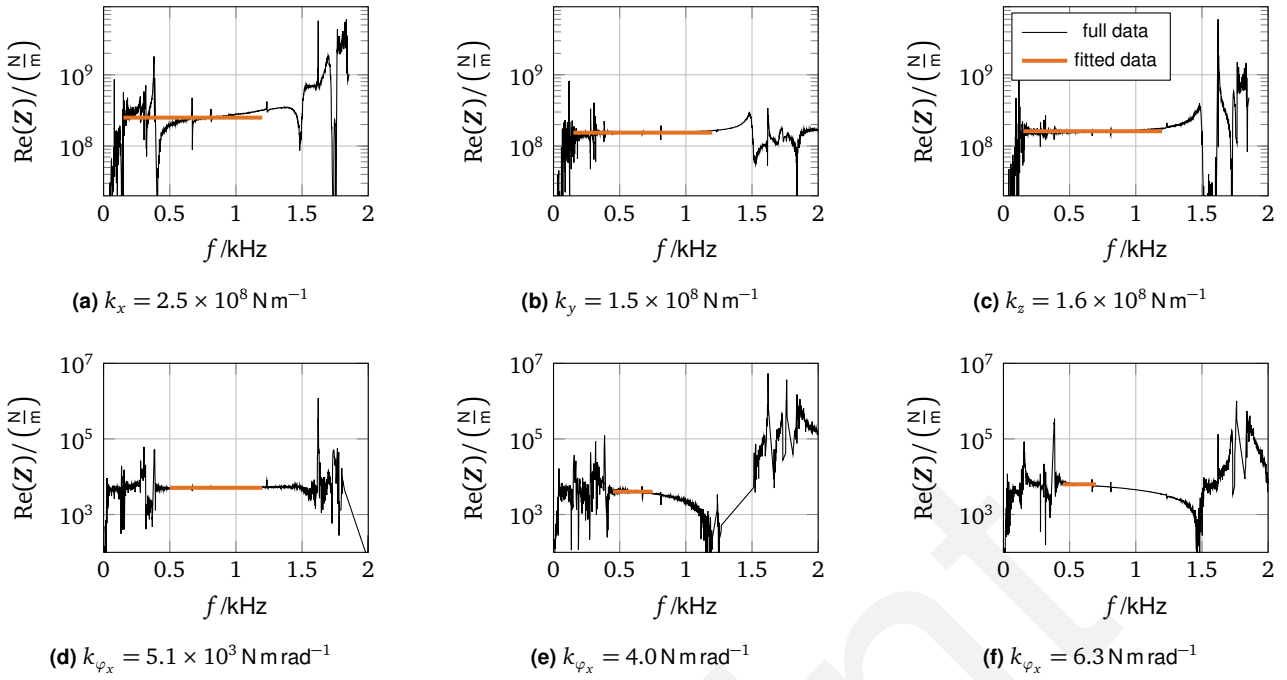


Figure 14: Parametrization of the direct stiffness.

in these directions or due to asymmetric behavior of the joint because of joint preload, e.g. by gravity.

3.3.2 Note about Damping

The identification of the damping fails in giving clear quantitative values. The imaginary part of Z is very close to zero and even crosses zero, switching signs, which indicates very low damping values. Due to this, the measurement noise has a rather large influence on the damping identification. Figure 15 shows damping identification for the z -direction exemplarily, which clearly gives unsatisfactory results.

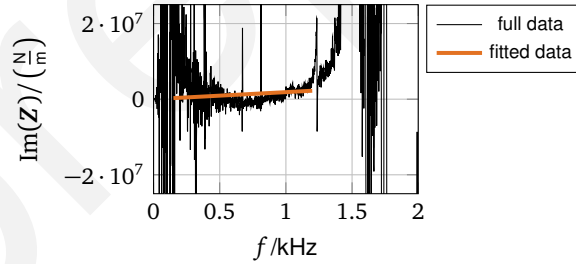


Figure 15: Example of damping identification for the z -direction.

The noise floor in an experimental setting will commonly hinder the identification of a very low damping. Damping values may still be retrieved if a further model updating procedure with a numerical approach is followed. However, doubts regarding the relevance of having such damping in the joint arise if these do not contribute significantly in the dynamics of the assembled system.

The low damping assumption can be validated by investigating the modal damping of the modes of the assembled system. The modal parameters are assessed from the VP-transformed FRF matrix of the assembled system Y_{qm}^{AJB} . Only the driving point FRF for excitation and response in x -direction are considered. An LSCF-identification (*Least-Squares Complex Frequency*) is used in the pyEMA-toolbox [17]. Figure 16 shows the amplitude of the considered FRF with the modal damping of the modes written near the corresponding peaks.

The damping values of the assembled system are very low, which concludes that the damping of the joint must also be very low.

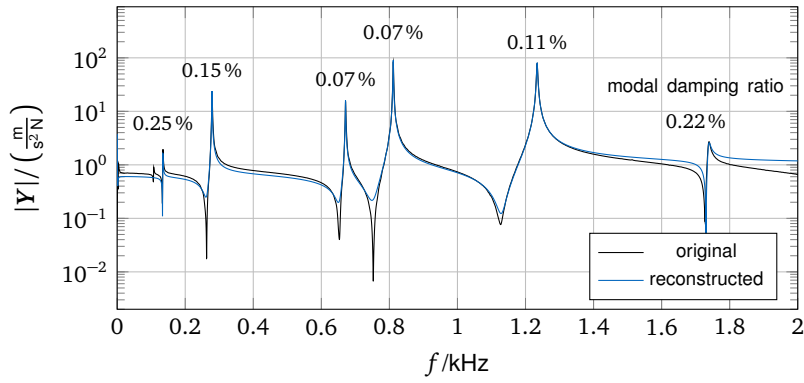


Figure 16: FRF-amplitude $|Y_{qm}^{AJB}|$ of the assembled system for excitation and response in x -direction with modal damping corresponding to the different peaks, here given as acceleration.

3.3.3 Repeatability

Repeatability is checked by comparing results on the system before and after a re-assembly. The isolation step with Inverse Substructuring and the parametrization step are repeated. The resulting stiffnesses are summarized in table 2.

Table 2: Identified joint stiffness for two measurement sets. The system was disassembled and reassembled between the measurements.

	stiffness first measurement set	stiffness second measurement set	change in stiffness
k_x	$2.50 \times 10^8 \text{ N m}^{-1}$	$3.08 \times 10^8 \text{ N m}^{-1}$	+23 %
k_y	$1.54 \times 10^8 \text{ N m}^{-1}$	$1.55 \times 10^8 \text{ N m}^{-1}$	+1 %
k_z	$1.61 \times 10^8 \text{ N m}^{-1}$	$1.59 \times 10^8 \text{ N m}^{-1}$	-1 %
k_{φ_x}	$5.10 \times 10^3 \text{ N m rad}^{-1}$	$4.66 \times 10^3 \text{ N m rad}^{-1}$	-8 %
k_{φ_y}	$4.02 \times 10^3 \text{ N m rad}^{-1}$	$4.97 \times 10^3 \text{ N m rad}^{-1}$	+24 %
k_{φ_z}	$6.30 \times 10^3 \text{ N m rad}^{-1}$	$5.67 \times 10^3 \text{ N m rad}^{-1}$	-10 %

It can be seen that repeatability of the translational dofs y and z (perpendicular to the bolt axis) is very good, while there are some differences in the other directions. This can be explained by the overall difficulties in clearly isolating and parametrizing the stiffness in these directions, which also has been commented in the previous sections.

3.3.4 Summary of the parametrization

The frequency range for the parametrization has to be selected manually, looking for clean regions in the identified dynamic stiffnesses. Estimation of the stiffness works very well for the translational directions, especially for y and z direction. Estimation for the rotational stiffnesses has larger uncertainty. The damping cannot be reliably estimated for the given case, as it appears to be too low and cannot be distinguished from other measurement uncertainties propagating through the substructuring procedure. More advanced methods, like model updating, are necessary to parametrize the damping, even if the distinction between joint and structure damping will be challenging for these scenarios. Here, the joint is parametrized as uncoupled three translational and three rotational stiffnesses without damping.

3.4 Validation

Here, the identified joint parameters and measurement of the substructures A , B are used to re-construct the assembled system FRFs using a primal coupling procedure similar to section 2.1.2. The results of the coupling are compared to measured FRFs of the assembly. This procedure is performed for the original system AJB and for a slightly modified system A^*JB .

3.4.1 Validation with Original System

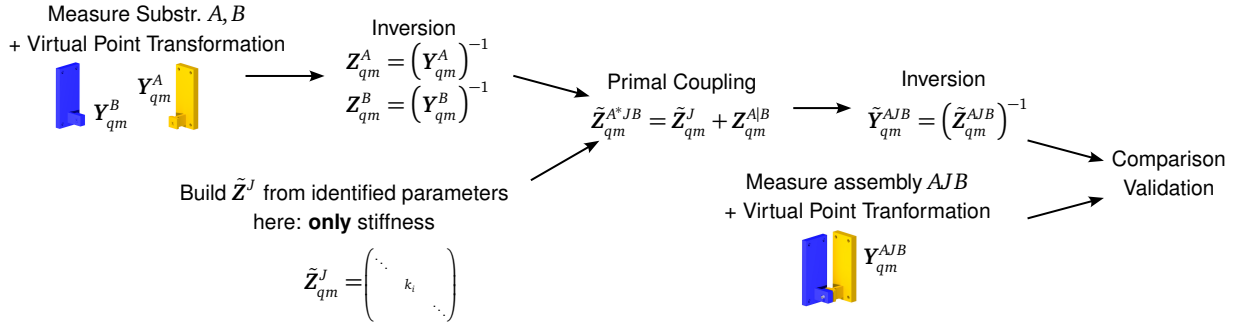


Figure 17: Procedure for validation.

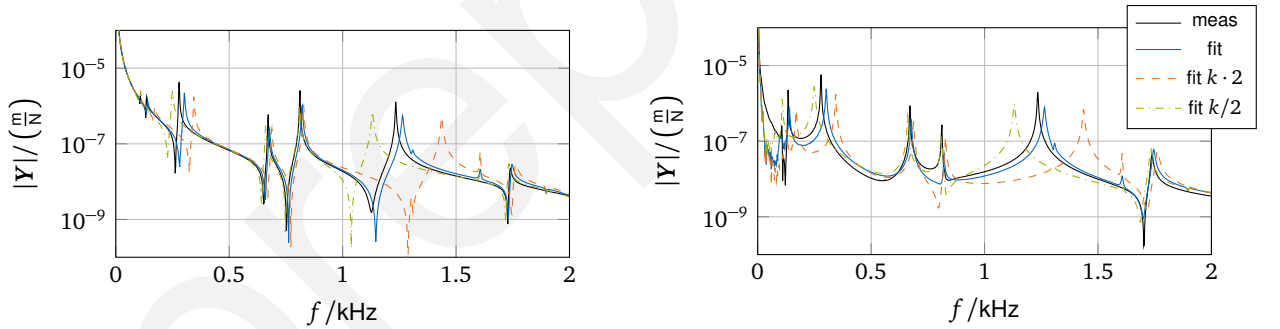
First, validation is performed using the original system AJB . See the summary of the procedure in fig. 17

The substructures A and B are measured individually and a VPT is performed. The FRFs are inverted to obtain the dynamic stiffnesses $\mathbf{Z}_{qm}^A, \mathbf{Z}_{qm}^B$. The stiffness matrix of the joint is called $\tilde{\mathbf{Z}}_{qm}^J$. These dynamic stiffness matrices are assembled by primal coupling. The resulting dynamic stiffness of the assembled system is inverted to obtain the FRFs in terms of the VP-coordinates: $\tilde{\mathbf{Y}}_{qm}^{AJB} = (\tilde{\mathbf{Z}}_{qm}^{AJB})^{-1}$.

These reconstructed FRFs are compared with the directly measured FRFs of the assembled system in terms of VP-coordinates \mathbf{Y}_{qm}^{AJB} .

To assess the robustness/validity of the isolated joint properties, the identified stiffnesses values are slightly changed and the new assembled predictions evaluated. For this, two additional reconstructed systems are built with a halved ($\tilde{\mathbf{Z}}_{qm, \text{half}}^J = \tilde{\mathbf{Z}}_{qm}^J / 2$) and doubled ($\tilde{\mathbf{Z}}_{qm, \text{double}}^J = 2 \cdot \tilde{\mathbf{Z}}_{qm}^J$) joint stiffness. If the identified joint dynamics are meaningful, the results should clearly worsen with the altered stiffness.

The magnitude of the FRFs are given as comparisons for different dofs in Figures 18a and 18b.



(a) diagonal-entry in x of \mathbf{Y}_{qm}^{AJB} (force in x - to displacement in x -direction).

(b) off-diagonal entry of \mathbf{Y}_{qm}^{AJB} – force in y - to displacement in x -direction.

Figure 18: Comparison of original measured FRF \mathbf{Y}_{qm}^{AJB} with reconstructed FRFs for validation.

It can be seen in figs. 18a and 18b that the reconstructed FRF is very close to the measured FRF. Furthermore, the joint stiffness deviations with factor two, half or double, show definitely worse prediction results.

This analysis also indicates that it would also be possible to further tune the values of the identified stiffnesses to have a better match between the reconstructed FRFs of \mathbf{Y}_{qm}^{AJB} and the measured once. However, the discrepancies seen in fig. 18 could also come from e.g. small measurements errors of the FRFs of A and B used in the assembly, it is not clear if a further tuning would truly yield more accurate joint parameters.

It is concluded that the reduction of the joint model to three translational and three rotational constant stiffnesses is acceptable. The damping of the joint is negligible, as it does not significantly contribute to the damping of the assembly.

3.4.2 Cross-Validation with Altered System

Now, substructure A is slightly changed by adding an additional mass to it. The new substructure is called A^* , see fig. 20a. In fig. 20b, lower eigenfrequencies of A^*JB can be seen compared to AJB , the change is visible in every

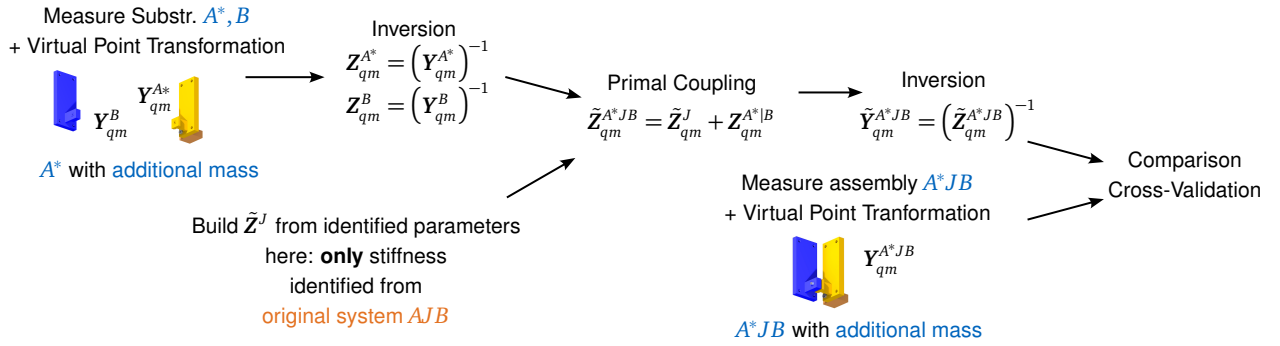
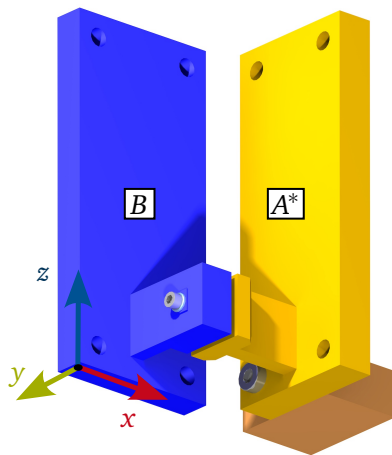
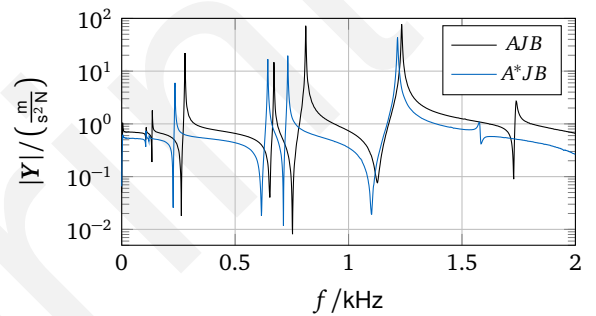


Figure 19: Procedure for cross-validation.



(a) Rendering of system A^*JB



(b) Amplitude of driving point FRF $Y_{qm}^{A^*JB}$ (here: acceleration) in x -direction: force in x - to acceleration in x -direction.

Figure 20: System A^*JB with additional mass added to substructure A .

peak. Overall dynamic behavior is still similar. The contact interface remains unchanged.

In the previous section, the identified dynamic stiffness \tilde{Z}^J (from AJB) was used to reconstruct AJB from substructures A and B with \tilde{Z}^J . Now, in the cross-validation the identified dynamic stiffness \tilde{Z}^J (from AJB) is used to reconstruct A^*JB from substructures A^* and B with \tilde{Z}^J . This procedure checks if the identified stiffness can be transferred to another system.

Figure 21 shows a comparison of the measured and reconstructed FRFs. The reconstructed $|Y_{qm}^{A^*JB}|$ is similar to the measured curve. In some non-driving point measurements, see fig. 21c, the anti-resonances are shifted or even skipped, which can be seen in the box in fig. 21c. In the which can be seen specifically. The resonance positions always agree well. For a scaling of the joint stiffness with a factor 2 the correlation between the reconstructed system and the measured one are clearly worse.

The transferability of the obtained joint parameters has been validated. The identified joint dynamics is truly a property of the joint alone, independent from the substructures. However, the system used for cross-validation was only slightly modified from the original system. An even stronger prove of the transferability would be the application of the identified joint parameters to a completely different system with the same bolted joint. Care must be taken that the joint parameters are the same in the new configuration. Many factors, like e.g. mass loading or preload of the interface, can influence the dynamics of the joint.

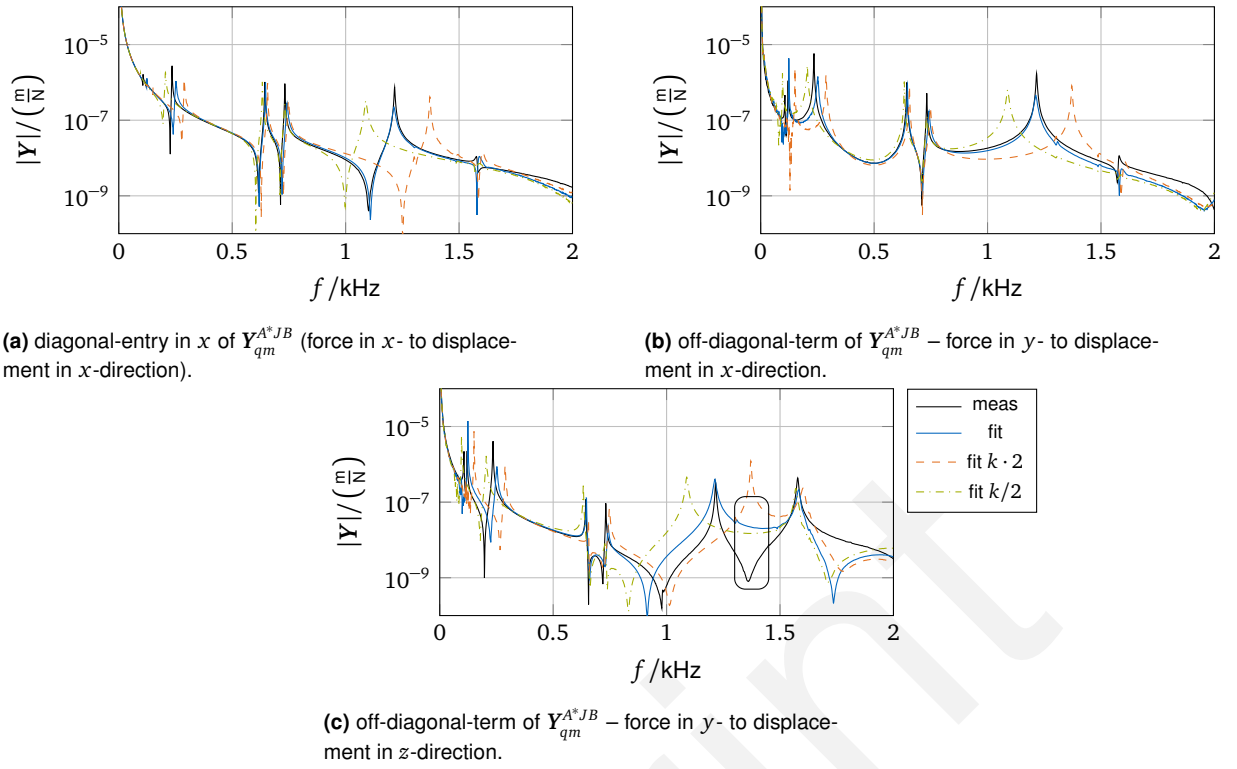


Figure 21: Comparison of measured FRF of the altered system Y_{qm}^{A*JB} with reconstructed FRFs for cross-validation.

3.5 Variation of the Bolt Torque

In a new experiment on the modified system A^*JB , the bolt torque is varied. Isolation results for the original torque level and for a significantly lower torque level ($M_{low} \approx M_{original}/3$) are compared. The results are presented in fig. 22, where the real part of the isolated joint FRFs are presented for the translational directions. The real part corresponds to the stiffness of the joint. The results for rotational dofs are not shown here, because these results are less clear.

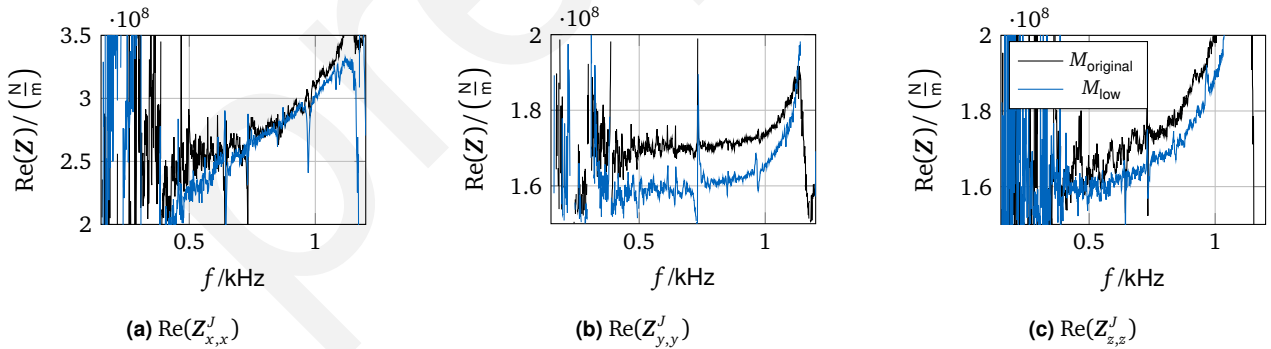


Figure 22: Real part of the isolated joint FRF for different torque levels

Stiffness in y and z -directions is lower for a lower bolt torque. A lower bolt torque reduces the preload in the bolted interface, which decreases the stiffness of the interface. But, the influence of the torque on the stiffness is still rather low, see the absolute values in fig. 22. For the stiffness in x -direction (along the bolt axis), there is no clear trend between torque and resulting joint stiffness. Since changes in impedance for the x -direction are in same order of magnitude of repeatability uncertainty, shown in section 3.3.3, no hard conclusion with the performed measurements can be made. The joint must be defined more strictly in the future to ensure good control.

4 Conclusion and Outlook

4.1 Conclusion

A robust procedure for the identification of bolted joints using frequency-based substructuring was presented on a real-life experimental application.

Inverse Substructuring gives good results for the analyzed case and only requires FRF measurements of the assembled system, but not of the individual substructures. The applicability of Inverse Substructuring was validated by a comparison with Primal Decoupling. The joint stiffness can be detected and identified. Damping can be considered as very small and was neglected in this case. In a validation step, it is shown that the original system can be well represented by the identified stiffness. In the cross-validation step, the transferability of the identified joint parameters to a slightly altered system is presented.

There are some limitations to the presented methodology. Low damping cannot be estimated quantitatively with the proposed isolation techniques. There is some uncertainty in the positioning of the impacts and sensors that can have an influence on the substructuring prediction, especially for rotational dofs. The effects of different torque levels was not assessed in details. There may be many effects that influence the joint stiffness that cannot be clearly separated yet, e.g. changing of the tribology due to assembly and disassembly or run-in effects. It is expected that preload of the joint has a larger influence, however, the preload-torque relationship is not clear.

4.2 Outlook

In further studies, the experimental procedure can be improved by using more sensors at the interface to improve the VPT and using an automatic impact hammer [14], to better control the impact positions. To get statistically relevant results for a parameter study, large measurement campaigns are necessary. A refined protocol for the experiments should be used to improve repeatability and to clearly isolate the effect of changes to different contact parameters.

To improve the decoupling, additional sensor data away from the interface, commonly called internal dofs [6, 25], can be used. More elaborate methods for decoupling can be used, like [23], which uses singular vector decomposition to smooth the processed measured data. Damping identification could be improved by model updating with a numerical model of the system, using the obtained stiffness and damping as a starting point for the optimization process, similar to [22].

CRedit authorship contribution statement: **M. Kreutz:** Conceptualization, Methodology, Software, Validation, Formal analysis, Investigation, Data curation, Writing - original draft, Writing - review & editing, Visualization. **F. Trainotti:** Conceptualization, Methodology, Investigation, Software, Writing - review & editing. **V. Gimpl:** Methodology, Software, Validation, Formal analysis, Investigation, Data curation. **D. J. Rixen:** Conceptualization, Resources, Writing - review & editing, Supervision.

Declaration of Competing Interest: The authors declare that they have no known competing financial interests or personal relationships that could have appeared to influence the work reported in this paper.

A Appendix: Detailed results

In the appendix, additional figures for the results presented above, are given. Figure 23 gives a comparison of Primal Decoupling and Inverse Substructuring results from sections 3.2.1 and 3.2.2.

Figure 24 shows the validation results from section 3.4 and fig. 25 shows the cross-validation results from section 3.4.2.

References

- [1] Allen, M. S., Rixen, D., Seijs, M. van der, Tiso, P., Abrahamsson, T., and Mayes, R. L. *Substructuring in Engineering Dynamics*. CISM International Centre for Mechanical Sciences. Cham: Springer International Publishing, 2020. ISBN: 978-3-030-25531-2. DOI: [10.1007/978-3-030-25532-9](https://doi.org/10.1007/978-3-030-25532-9).

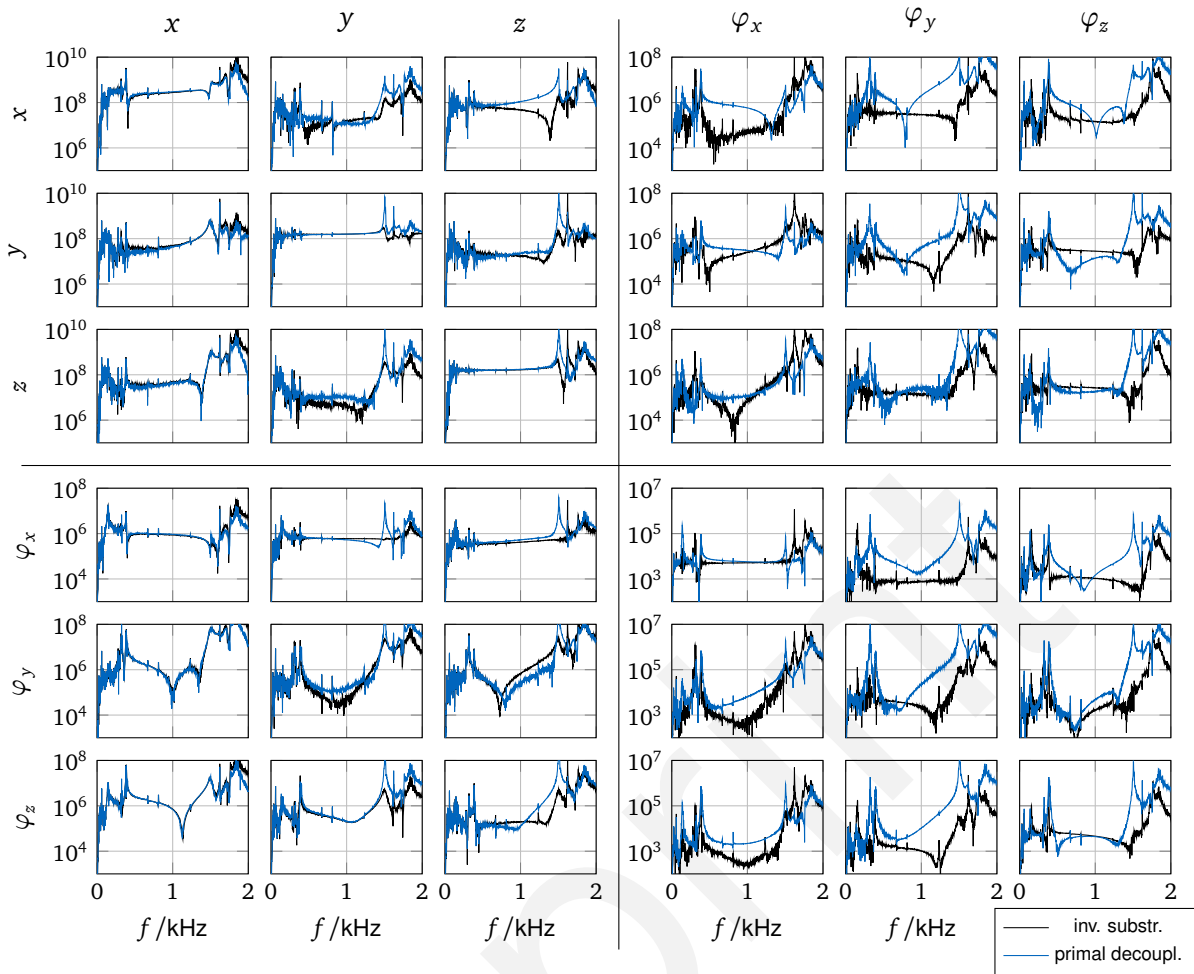


Figure 23: Primal Decoupling vs. Inverse Substructuring for all dofs: \mathbf{Z}_{qm}^J .

- [2] Barten, E., Van Der Seijs, M. V., and De Klerk, D. “A complex power approach to characterise joints in experimental dynamic substructuring”. In: *Conference Proceedings of the Society for Experimental Mechanics Series* 1.June (2014), pp. 281–296. ISSN: 21915652. DOI: [10.1007/978-3-319-04501-6_27](https://doi.org/10.1007/978-3-319-04501-6_27).
- [3] Bregar, T., Mahmoudi, A., Kodrič, M., Ocepek, D., Trainotti, F., Pogačar, M., Gödeli, M., Čepon, G., Boltežar, M., and Rixen, D. “pyFBS: A Python package for Frequency Based Substructuring”. In: *Journal of Open Source Software* 7.69 (2022), p. 3399. DOI: [10.21105/joss.03399](https://doi.org/10.21105/joss.03399).
- [4] Brunetti, J., D’Ambrogio, W., Manno, M. D., Fregolent, A., and Latini, F. “Identification of Bolted Joint Properties Through Substructure Decoupling”. In: *Dynamic Substructures*. Vol. 4. Springer International Publishing, 2023, pp. 85–95. DOI: [10.1007/978-3-031-04094-8_11](https://doi.org/10.1007/978-3-031-04094-8_11).
- [5] Čelič, D. and Boltežar, M. “Identification of the dynamic properties of joints using frequency-response functions”. In: *Journal of Sound and Vibration* 317.1-2 (2008), pp. 158–174. ISSN: 0022460X. DOI: [10.1016/j.jsv.2008.03.009](https://doi.org/10.1016/j.jsv.2008.03.009).
- [6] D’Ambrogio, W. and Fregolent, A. “Decoupling procedures in the general framework of Frequency Based Substructuring”. In: *Conference Proceedings of the Society for Experimental Mechanics Series* May (2009). ISSN: 21915644.
- [7] De Klerk, D., Rixen, D. J., and Voormeeren, S. N. “General framework for dynamic substructuring: History, review, and classification of techniques”. In: *AIAA Journal* 46.5 (2008), pp. 1169–1181. ISSN: 00011452. DOI: [10.2514/1.33274](https://doi.org/10.2514/1.33274).
- [8] De Klerk, D., Rixen, D. J., and De Jong, J. “The Frequency Based Substructuring (FBS) method reformulated according to the dual Domain Decomposition method”. In: *Conference Proceedings of the Society for Experimental Mechanics Series* January 2006 (2006). ISSN: 21915644.

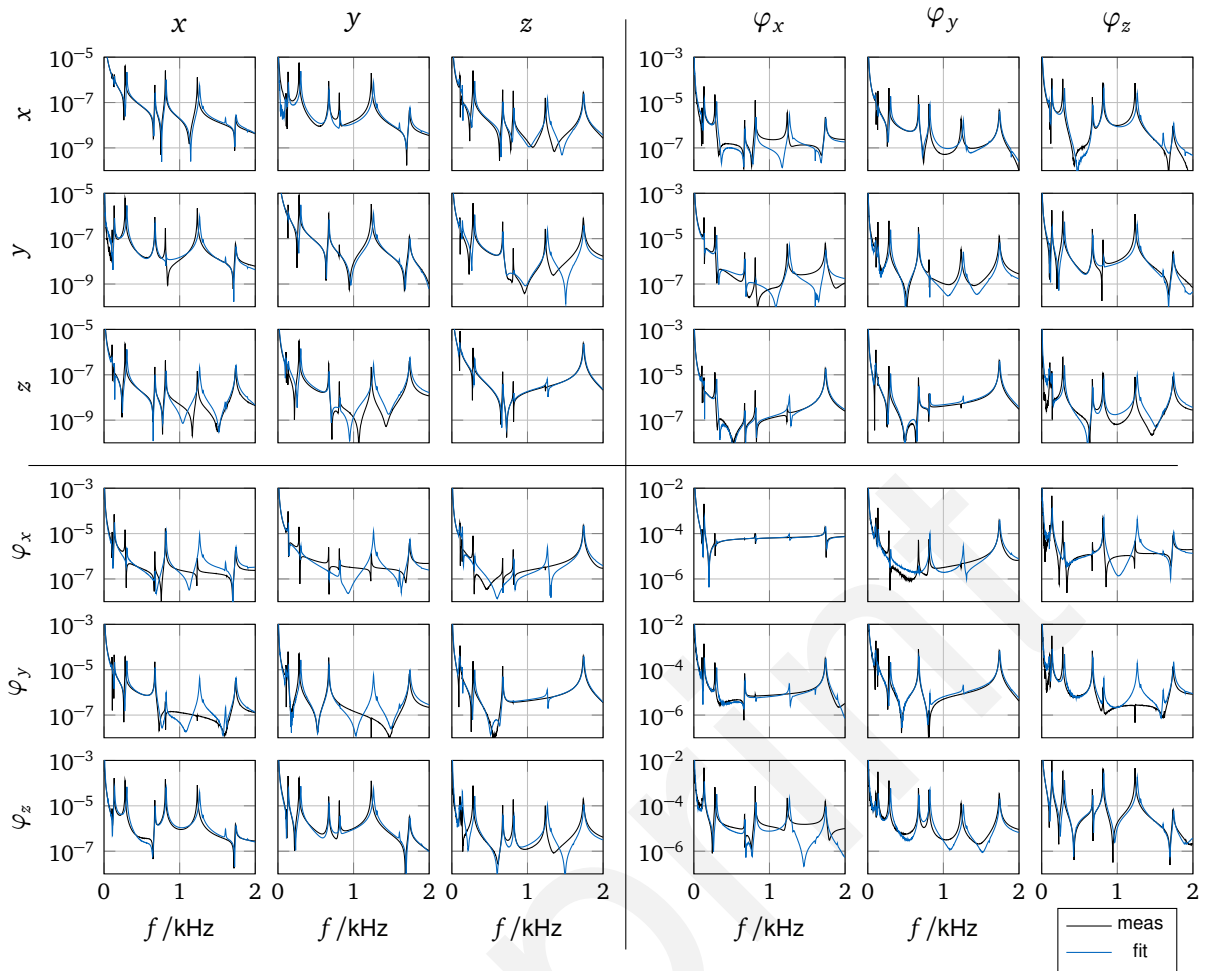


Figure 24: Validation for all dofs: \mathbf{Y}_{qm}^{AJB} .

- [9] Gimpl, V., Fantetti, A., Klaassen, S. W., Schwingshackl, C. W., and Rixen, D. J. “Contact stiffness of jointed interfaces: A comparison of dynamic substructuring techniques with frictional hysteresis measurements”. In: *Mechanical Systems and Signal Processing* 171. September 2021 (2022), p. 108896. ISSN: 10961216. DOI: [10.1016/j.ymsp.2022.108896](https://doi.org/10.1016/j.ymsp.2022.108896).
- [10] Häußler, M., Klaassen, S., and Rixen, D. “Experimental twelve degree of freedom rubber isolator models for use in substructuring assemblies”. In: *Journal of Sound and Vibration* 474 (May 2020). ISSN: 0022460X. DOI: [10.1016/j.jsv.2020.115253](https://doi.org/10.1016/j.jsv.2020.115253).
- [11] Häußler, M. and Rixen, D. J. “Optimal Transformation of Frequency Response Functions on Interface Deformation Modes”. In: *Conference Proceedings of the Society for Experimental Mechanics Series*. 2017, pp. 225–237. ISBN: 9783319549293. DOI: [10.1007/978-3-319-54930-9_20](https://doi.org/10.1007/978-3-319-54930-9_20).
- [12] Keersmaekers, L., Mertens, L., Penne, R., Guillaume, P., and Steenackers, G. “Decoupling of mechanical systems based on in-situ frequency response functions: The link-preserving, decoupling method”. In: *Mechanical Systems and Signal Processing* 58-59.2015 (June 2015), pp. 340–354. ISSN: 08883270. DOI: [10.1016/j.ymsp.2014.11.016](https://doi.org/10.1016/j.ymsp.2014.11.016).
- [13] Klaassen, S., Cigeroglu, E., and Özgüven, H. N. “Identifying the joint dynamics of a bolted beam system by using FRF decoupling and the SEMM expansion technique”. In: *Tribomechadynamics* (2019).
- [14] Maierhofer, J., Mahmoudi, A. E., and Rixen, D. J. “Development of a Low Cost Automatic Modal Hammer for Applications in Substructuring”. In: *Conference Proceedings of the Society for Experimental Mechanics Series*. Vol. 4. 2020, pp. 77–86. ISBN: 9783030121839. DOI: [10.1007/978-3-030-12184-6_9](https://doi.org/10.1007/978-3-030-12184-6_9).
- [15] Meggitt, J. W. and Moorhouse, A. T. “In-situ sub-structure decoupling of resiliently coupled assemblies”. In: *Mechanical Systems and Signal Processing* 117. August (2019), pp. 723–737. ISSN: 10961216. DOI: [10.1016/j.ymsp.2018.07.045](https://doi.org/10.1016/j.ymsp.2018.07.045).

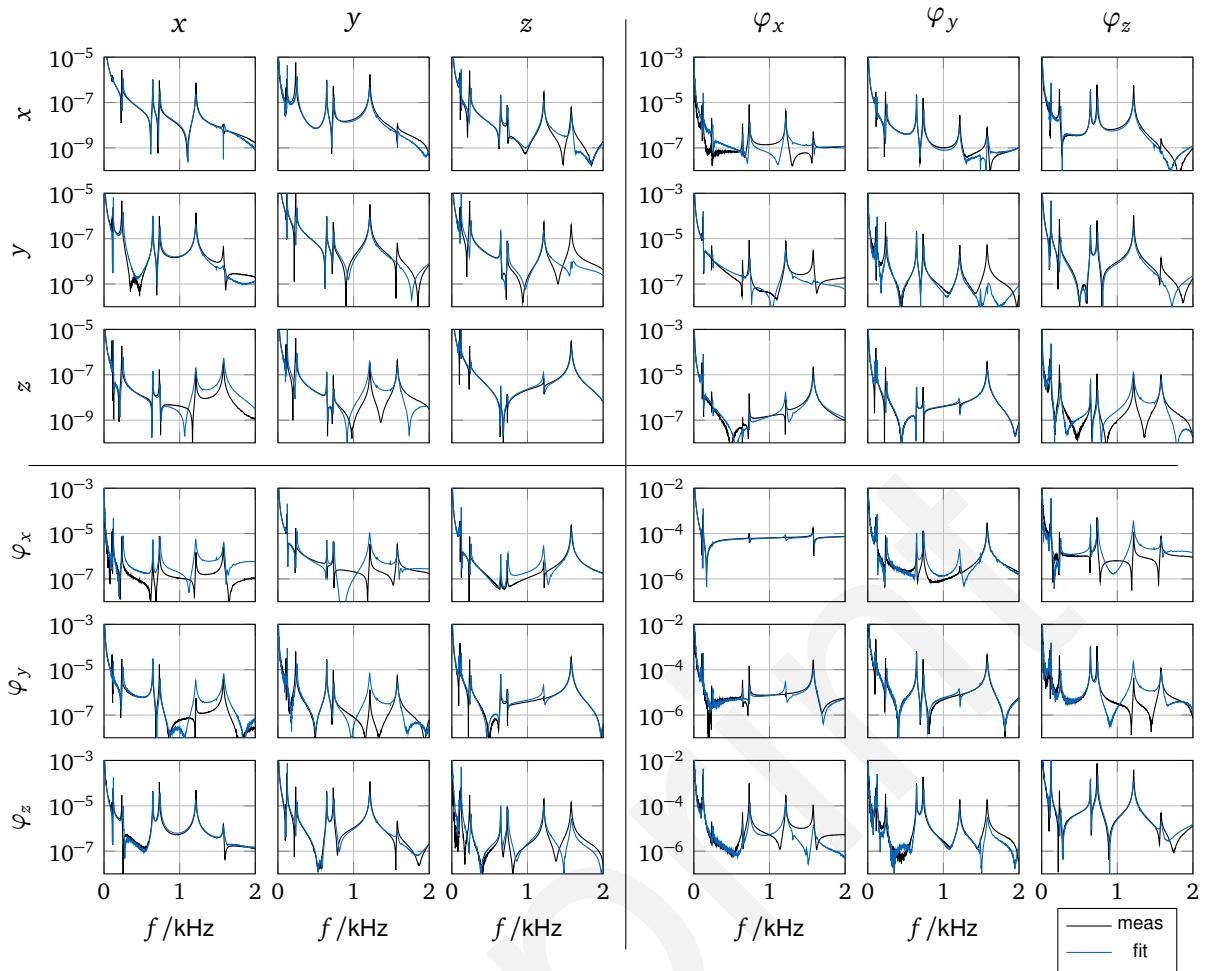


Figure 25: Cross-Validation for all dofs: Y_{qm}^{A*JB} .

- [16] Meggitt, J., Elliott, A., Moorhouse, A., and Lai, H. K. "In situ determination of dynamic stiffness for resilient elements". In: *Proceedings of the Institution of Mechanical Engineers, Part C: Journal of Mechanical Engineering Science* 230.6 (Apr. 2016), pp. 986–993. ISSN: 0954-4062. DOI: [10.1177/0954406215618986](https://doi.org/10.1177/0954406215618986).
- [17] *pyEMA - Github*. 2022. URL: <https://github.com/ladisk/pyEMA> (visited on 06/10/2022).
- [18] Ren, Y. and Beards, C. F. "Identification of joint properties of a structure using FRF data". In: *Journal of Sound and Vibration* 186.4 (1995), pp. 567–587. ISSN: 10958568. DOI: [10.1006/jsvi.1995.0469](https://doi.org/10.1006/jsvi.1995.0469).
- [19] Seijs, M. van der. "Experimental Dynamic Substructuring: Analysis and Design Strategies for Vehicle Development". Dissertation. Technische Universiteit Delft, 2016. ISBN: 9789461866714. DOI: [10.4233/uuid:28b31294-8d53-49eb-b108-284b63edf670](https://doi.org/10.4233/uuid:28b31294-8d53-49eb-b108-284b63edf670).
- [20] Seijs, M. V. van der, Klerk, D. de, and Rixen, D. J. "General framework for transfer path analysis: History, theory and classification of techniques". In: *Mechanical Systems and Signal Processing* 68-69 (2016), pp. 217–244. ISSN: 10961216. DOI: [10.1016/j.ymssp.2015.08.004](https://doi.org/10.1016/j.ymssp.2015.08.004).
- [21] Sjövall, P. and Abrahamsson, T. "Substructure system identification from coupled system test data". In: *Mechanical Systems and Signal Processing* 22.1 (Jan. 2008), pp. 15–33. ISSN: 08883270. DOI: [10.1016/j.ymssp.2007.06.003](https://doi.org/10.1016/j.ymssp.2007.06.003).
- [22] Tol, . and Özgüven, H. N. "Dynamic characterization of bolted joints using FRF decoupling and optimization". In: *Mechanical Systems and Signal Processing* 54 (2015), pp. 124–138. ISSN: 10961216. DOI: [10.1016/j.ymssp.2014.08.005](https://doi.org/10.1016/j.ymssp.2014.08.005).
- [23] Trainotti, F., Bregar, T., Klaassen, S., and Rixen, D. "Experimental decoupling of substructures by singular vector transformation". In: *Mechanical Systems and Signal Processing* 163.June 2021 (Jan. 2022). ISSN: 08883270. DOI: [10.1016/j.ymssp.2021.108092](https://doi.org/10.1016/j.ymssp.2021.108092).

- [24] Van Der Seijs, M. V., Van Den Bosch, D. D., Rixen, D. J., and De Klerk, D. "An improved methodology for the virtual point transformation of measured frequency response functions in Dynamic Substructuring". In: *ECCOMAS Thematic Conference - COMPDYN 2013: 4th International Conference on Computational Methods in Structural Dynamics and Earthquake Engineering, Proceedings - An IACM Special Interest Conference* June (2013), pp. 4334–4347. DOI: [10.7712/120113.4816.c1539](https://doi.org/10.7712/120113.4816.c1539).
- [25] Voormeeren, S. and Rixen, D. "A family of substructure decoupling techniques based on a dual assembly approach". In: *Mechanical Systems and Signal Processing* 27 (Feb. 2012), pp. 379–396. ISSN: 08883270. DOI: [10.1016/j.ymsp.2011.07.028](https://doi.org/10.1016/j.ymsp.2011.07.028).
- [26] Wang, Z. W. and Jun Wang. "Inverse substructure method of three-substructures coupled system and its application in product-transport-system". In: *JVC/Journal of Vibration and Control* 17.6 (2011), pp. 943–952. ISSN: 10775463. DOI: [10.1177/1077546310376083](https://doi.org/10.1177/1077546310376083).

preprint